Journal of Civil Structural Health Monitoring (2023) 13:117–132
https://doi.org/10.1007/s13349-022-00626-9

ORIGINAL PAPER

Experimental investigation and damage evaluation of a novel bond type anchorage for carbon fiber reinforced polymer tendons

Shiyuan Ju[1] · Dongsheng Li[1] · Jinqing Jia[1]

Received: 22 April 2022 / Accepted: 23 August 2022 / Published online: 3 September 2022

Abstract
The bond type anchorage is most suitable for anchoring carbon fiber reinforced polymer (CFRP) tendons, but its shape causes stress concentration. In addition, the failure modes of bonded anchors are difficult to observe and the damage process is difficult to analyze. The aim of this study was to address the above problems. To relieve the stress concentration, a novel arcuate-cone bond type anchorage was designed in this study. The failure modes and load-slip curves were obtained by tension tests on a group of anchors. The test results indicated that the stress concentration can be effectively alleviated. Acoustic emission technique was used to monitor the damage process of bond type anchorages under tension load. By analyzing the acoustic emission data, the damage process of bond type anchorage can be divided into three stages and the different failure modes can be identified. Finally, the failure mechanism of bonded anchorages was discussed based on the test results and monitoring data.

Keywords Bond type anchorage · CFRP tendon · Tension test · Arcuate-cone anchorage · Acoustic emission

1 Introduction

Carbon fiber-reinforced polymer (CFRP) is a new type of material widely used in civil engineering because of its low weight, high tensile strength, and corrosion resistance [1–3]. Therefore, CFRP tendons or cables are the best substitutes for steel. Unlike steel, the transverse shear strength of CFRP is significantly lower than its axial tensile strength [4]. The difference in material properties makes it impossible to directly apply conventional anchors for anchoring steel bars to CFRP tendons. Consequently, it is necessary to design a new anchorage system for CFRP tendons. Many researchers believe that the stress concentrations occurring in the anchorage zone will lead to cut-off of the CFRP tendons and will not be able to perform the load-bearing capacity of the tendons [5–8]. Therefore, they studied mechanical anchorages and bond type anchorages in order to solve this problem.

The mechanical anchorage is composed of a steel barrel and metal wedges [9]. Its important disadvantages are the tendon's susceptibility to damage and the presence of stress concentrations [10]. The components of the bond type anchorage are a steel barrel, filling materials, and CFRP tendons [11]. As the filling materials and CFRP tendons are solidified together, the tendons anchored with bond type anchorages do not damage. Since the colloid in the bonded anchorage is similar to the CFRP tendon matrix, the two work better together. Many different types of bonded anchors have been developed, as shown in Fig. 1. However, stress concentration also occurs in conventional inner cone bond type anchors at the loading end. For FRP materials, stress concentrations will lead to premature failure of the tendons before ultimate tensile strength can be reached, especially in anchors with high stiffness [12, 13]. To avoid premature failure of FRP tendons, many researchers have proposed different methods for relieving stress concentrations in anchorages.

Campbell et al. designed a wedge anchorage with an angle difference between the barrel and metal wedges and experimentally analyzed its mechanical properties [5]. Meier and Farshad found that using variable stiffness material as colloid obtains uniform stress distribution [6]. Considering the complexity of Meier's approach, Mei et al. proposed a new method to solve this problem by changing the shape of barrel, and carried out a series of experimental studies [7, 8].

✉ Dongsheng Li
lidongsheng@dlut.edu.cn

[1] School of Civil Engineering, Dalian University of Technology, 2 Linggong Road, Dalian, China

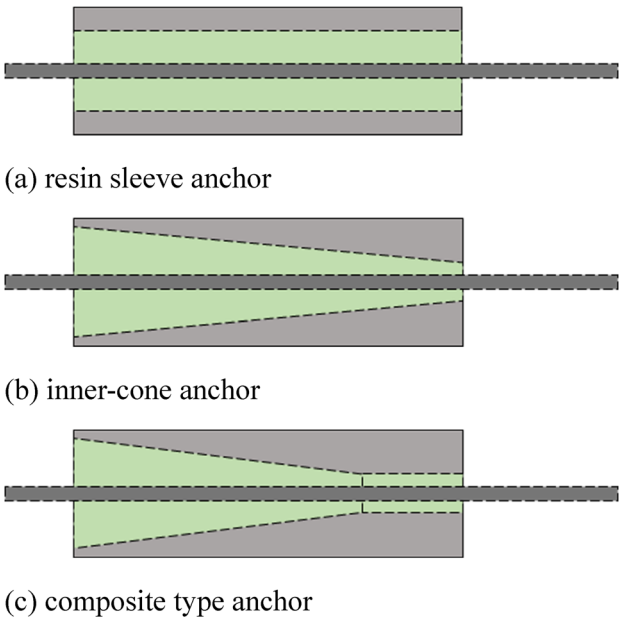

Fig. 1 Different types of bonded anchors

Despite the availability of many different types of anchorages, stress concentrations in the anchorage zone still exist and limit the performance of CFRP tendons. To relieve the stress concentration phenomenon, the authors designed a novel bonded anchorage.

In addition to the problem caused by the stress concentration phenomenon, there are two other problems to be solved:

(1) The bonded anchorage has a variety of failure modes, which are difficult to observe in engineering applications,
(2) The damage process is difficult to analyze because the filling materials are wrapped in the barrel.

Nevertheless, previous studies mostly focused on the mechanical properties and bearing capacity of anchorage, and a few studies investigated its failure mechanism. To address the two problems requires the development of a non-destructive health monitoring method to analyze the failure mechanism of CFRP bond type anchorages.

Acoustic emission (AE) technique has been widely used as a non-destructive testing (NDT) technique in structural health monitoring and damage evaluation [14–17]. So far, the application of acoustic emission technique in concrete structure health monitoring has been mature [18–20]. When plastic deformation or cracks occur under load, the energy is released in the form of stress waves [21]. Acoustic emission technique converts these waves into electrical signals (AE signals) and extracts damage-related information from them. When compared with other NDT techniques, AE technique is more sensitive to minor damage and has a larger monitoring area; hence, it does not pre-judge the damage location [22]. Owing to the aforementioned advantages, AE technique is very suitable for monitoring the damage process of fiber reinforced polymer (FRP) materials with numerous minor damages. Thus far, studies have proved that it is feasible to use AE technology to monitor the damage of FRP materials [23, 24].

In this paper, a series of studies are conducted based on three problems of bonded anchorages and the task flowchart is shown in Fig. 2. In this study, a novel arcuate-cone bond type anchorage was designed to alleviate the stress concentration phenomenon. The failure modes, ultimate bearing capacity and load-slip curves were obtained by the tension test. In addition, AE technique was used to monitor the damage process of a group of bonded anchorages, to identify different failure modes of bond type anchorages.

2 Experimental procedure

2.1 Specimen preparation

The specimens for tension tests can be divided into two categories: conventional inner-cone anchorage and novel arcuate-cone anchorage. The inner cone anchorage is the main form of bonded anchorage currently applied in engineering, but it leads to an inhomogeneous distribution of bonding stress on the surface of CFRP tendons, stress concentration, and premature failure of tendons. To solve this problem, the author designed a new arcuate-cone bonded anchorage based on the conventional anchorage by changing the internal shape of the steel barrel. The sections of the two anchorages are shown in Fig. 3, in which the parameters are marked.

As shown in Fig. 3, the inner surface of the conventional anchorage is a straight line, while that of the arcuate-cone anchorage is an arc. In Fig. 3, R represents the radius of the arc, and γ represents the inclination angle. The inner cone anchorages were labeled as "IC + bond length + (tanγ)," and arcuate-cone anchors were labeled as "AC + bond length + (tanγ)." To improve the generalizability of the test results and to ensure that the test results are not affected by specific anchorage parameters, eight different anchorages were designed in this study by changing the anchorage parameters. Two anchors with the same parameters of each label were tensioned, where the test result of the first broken anchorage was taken as the test result of that label. The labels of each anchorage and its corresponding parameters are listed in Table 1.

The structure of the bonded anchorage is simple and mainly consists of a steel barrel, filling materials, and CFRP tendons. The barrel used in this test was a steel

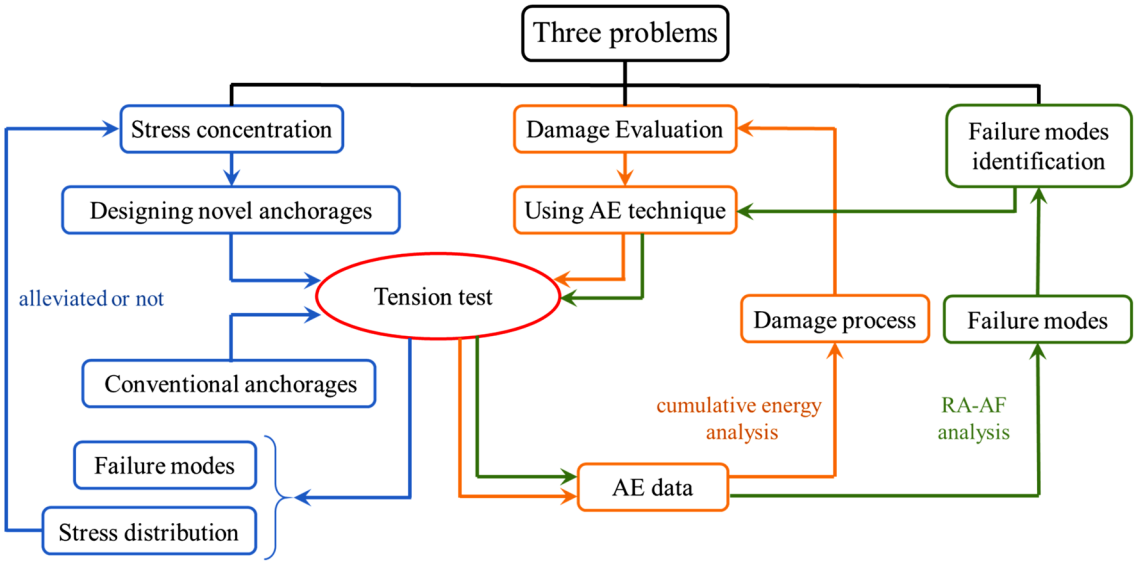

Fig. 2 Task flowchart of the present study

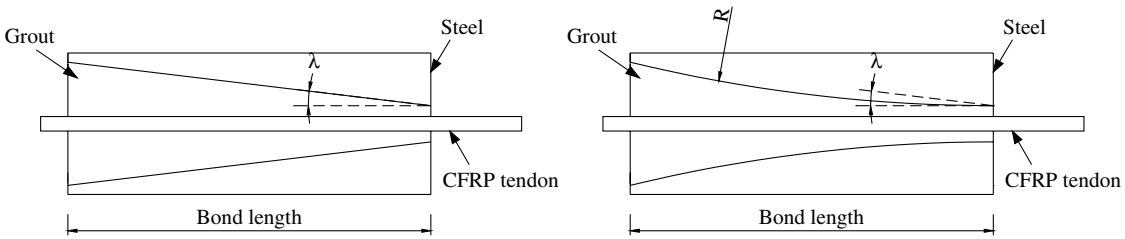

Fig. 3 Sections of two types of anchorages

Table 1 Label and parameters of each anchorage

Label	Type of anchor	Bond length (mm)	Tangential value of inclination angle	Radius (mm)
IC200(0.09)	Inner-cone	200	0.09	–
IC200(0.06)	Inner-cone	200	0.06	–
IC300(0.09)	Inner-cone	300	0.09	–
IC300(0.06)	Inner-cone	300	0.06	–
AC200(0.09)	Arcuate-cone	200	0.09	1,120
AC200(0.06)	Arcuate-cone	200	0.06	1,675
AC300(0.09)	Arcuate-cone	300	0.09	1,680
AC300(0.06)	Arcuate-cone	300	0.06	2,655

Q345. Q345 steel is a Chinese GB standard Low Alloy High Strength Structural Steel, its material density is 7.85 g/cm^3, yield strength is 345 MPa, ultimate tensile strength is 470–630 MPa. A Lica 300 epoxy resin adhesive produced by *Nanjing Hitech Composites Company* was used as the filling material because of its low elastic modulus, and CFRP tendons with a diameter of 8 mm were also manufactured by this company. The properties of each material were measured by the manufacturer through standard tests. Detailed material properties are listed in Table 2.

The specimen preparation process is categorized as material handling, component assembly, and curing of the bonding material. Material handling includes attaching strain gauges to the surface of CFRP tendons, cleaning the inner surface of the steel barrel with alcohol, and spraying epoxy resin release agent on it. Component assembly

Table 2 Material parameters of specimen

Material	Tensile strength (MPa)	Compressive strength (MPa)	Elastic modulus (GPa)	Axial Poisson's ratio	Radial Poisson's ratio
CFRP tendons	2,000	–	140	0.27	0.02
Lica300 adhesive	40.1	73.6	2.61	0.25	0.25
steel	345	345	206	0.3	0.3

includes assembling the barrel and CFRP tendon together, and then pouring Lica 300 epoxy resin into the steel barrel using a glue injection gun. In the last step, the colloid should be cured naturally for 24 h at 25 °C, then wrapped around the barrel using a heating plate, and the epoxy resin should be cured for 5 h at 80 °C to achieve the designed strength. The assembly and preparation process of the specimens are shown in Fig. 4.

2.2 Test setup and procedure

The specimens were tested using a jack, and the load was graded at a speed of 5 kN per stage. The failure sign of the specimen is that the bearing capacity of the anchorages suddenly decreases or the slip increases instantaneously.

The values of the load, axial stress of tendons, and slip of the CFRP tendon relative to the anchorage should be obtained in tension tests of specimens. During the test, the load was measured using a pressure sensor, axial stress was measured using a strain gauge installed on the surface of tendons, and slip of the CFRP tendon was estimated using dial indicators; all data were recorded using a DongHua3820 signal acquisition instrument.

The acoustic emission (AE) signals during the test were collected using the *Physical Acoustics Corporation's* eight-channel signal monitoring system. An R15a acoustic emission sensor is connected at the end of each anchorage, which is further connected to the AE signal monitoring system through a preamplifier. To ensure the accuracy of the AE data, Vaseline was used as a coupling agent between the AE sensor and specimen. The pencil-lead break procedure was conducted before the formal tension test. The schematic diagram of the test setup and AE system is shown in Fig. 5.

3 Test results and discussion

3.1 Failure modes

There are three different failure modes of bonded anchorage, including pull-out failure, partial debonding failure, and tensile fracture of the CFRP tendons, which are shown (a)–(c) in Fig. 6. Different anchorage parameters lead to different failure modes; the failure modes of each specimen are listed in Table 3.

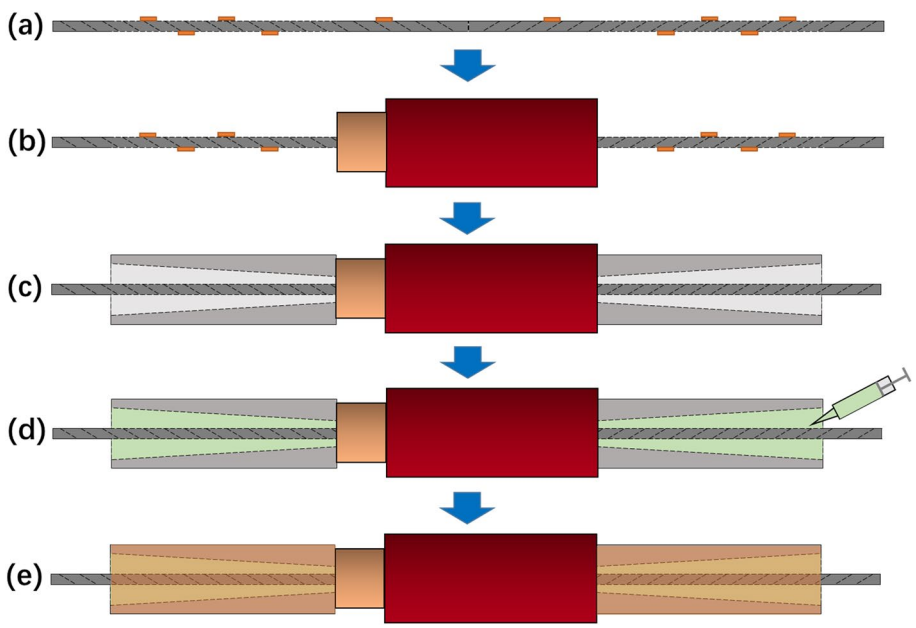

Fig. 4 Specimen preparation process **a** strain gauge attachment **b** tendons through the loading device **c** anchorage assembly **d** injection of epoxy resin **e** heating and curing

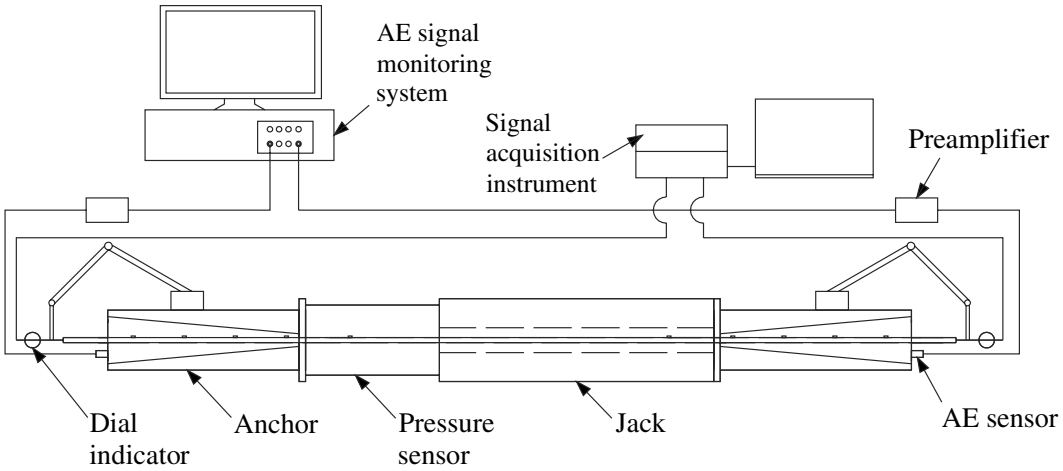

(a) Schematic diagram of test setup

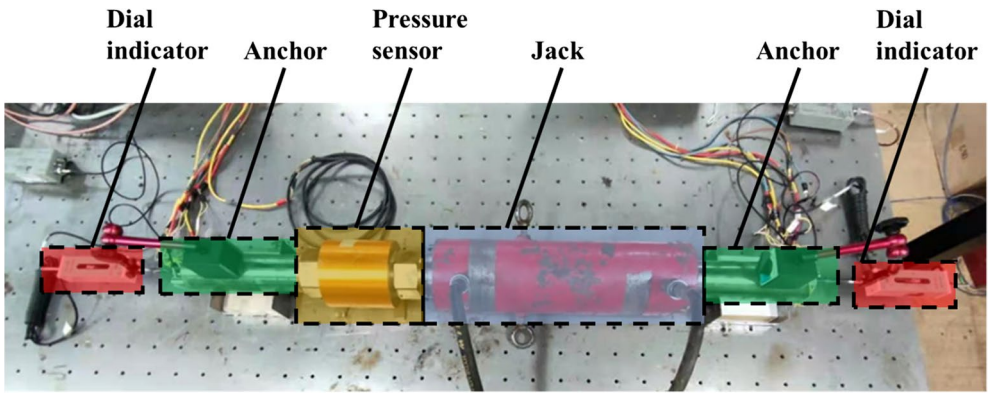

(b) Each part of test setup

Fig. 5 Testing setups and monitoring system of anchorages

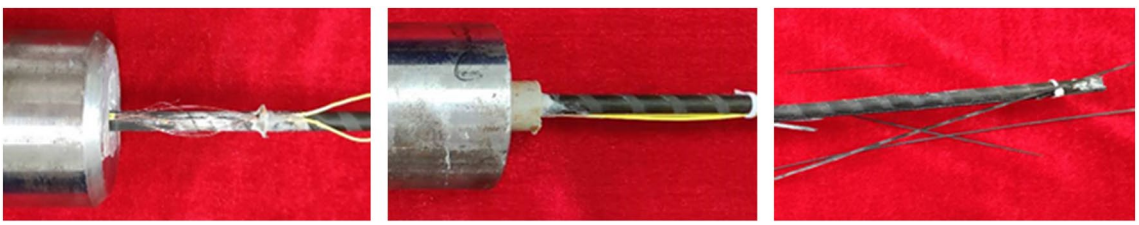

Fig. 6 Three failure modes **a** pull-out failure **b** partial debonding failure **c** tensile fracture

Among the three failure modes, pull-out failure is the most common, which is caused by the relative slip of the interface between the tendons and filling materials. However, the optimal failure mode is the tensile fracture of CFRP tendons, which indicates that the tensile strength of CFRP is completely utilized.

3.2 Load–slip relationship of anchorages

The slip in the load–slip curve refers to the slip of the CFRP tendon relative to the steel barrel during the formal loading process. Simultaneously, it can be divided into two parts: the slip of reinforcement relative to the filling material, and

Table 3 Failure modes of specimen

Label	Failure mode
IC200(0.09)	Pull-out failure
IC200(0.06)	Partial debonding failure
IC300(0.09)	Pull-out failure
IC300(0.06)	Pull-out failure
AC200(0.09)	Partial debonding failure
AC200(0.06)	Partial debonding failure
AC300(0.09)	Pull-out failure
AC300(0.06)	Tensile fracture of CFRP tendons

the slip of the filling material relative to the barrel. The former occurs immediately prior to specimen failure, while the latter continues to grow throughout the loading process. In the existing literature on anchorages, the load–slip curve is commonly used to describe the mechanical properties of bond type anchors [7, 8, 25–27].

The load–slip curves of different bonded anchorages obtained by tensioning tests are shown in Fig. 7. It is obvious from the figure that the load – slip curves of each specimen are nonlinear. At the lower load stage, the slip increases approximately linearly with the increase in load. However, when the load is about to reach the ultimate anchoring capacity, the slip rapidly increases. In addition, the slope of the load−slip curve reflects the slip degree of the colloid relative to the barrel under the same load. Figure 7 compares the load−slip curves of each specimen and shows that the anchorage with a smaller slope at the initial stage of loading has a greater ultimate anchoring capacity.

Some researchers have also performed tension tests on bonded anchorages. Mei et al. conducted a set of tensile tests of bonded anchorage and published the results in the article "Experimental investigation on the mechanical properties of a bond-type anchor for carbon fiber reinforced polymer tendons" [7]. Mei et al. produced three types of anchors, which were straight-type, inner cone type and composite-type. The specific test parameters can be found in reference 7. The anchorages in Mei's tests were different from the type of anchorages in the present study, but were similar in size. Therefore, the load–slip curves obtained experimentally by Mei et al. were also shown in Fig. 7 as a comparison. The straight, inner cone and composite anchors with a length of 300 mm were labeled as ZT300, NZ300 and FH300, and FH300S means that the tendon of this specimen has a scattered-end.

For specimens with pull-out failure, the ultimate bearing capacity obtained in this test was similar to the Mei's results. It can be inferred that the effect of anchorage type on the ultimate bearing capacity is not significant. This is because the arcuate-cone anchorage was designed to relieve stress concentration, that is, to avoid premature failure, which did not occur in the present test. Premature failure of tendons due to stress concentration often occurs in anchorages with high material stiffness, such as bonded anchorages with concrete mortar as filling material or mechanical anchorages with steel as wedge [25]. In the present test, epoxy resin was used as the filling material, whose stiffness was so low that premature failure did not occur.

The slope of the load–slip curve indicates the tendon slip under the same load. Obviously, the slips of the tendons obtained in the present test were significantly less than those of common anchors in Mei's test. While the slope of specimen FH300S in Mei's test is more similar to the present study. This is because an epoxy resin release agent was sprayed on the inner surface of the barrel in this test, so that the cone can slide relative to the barrel. The slip between the cone and the barrel

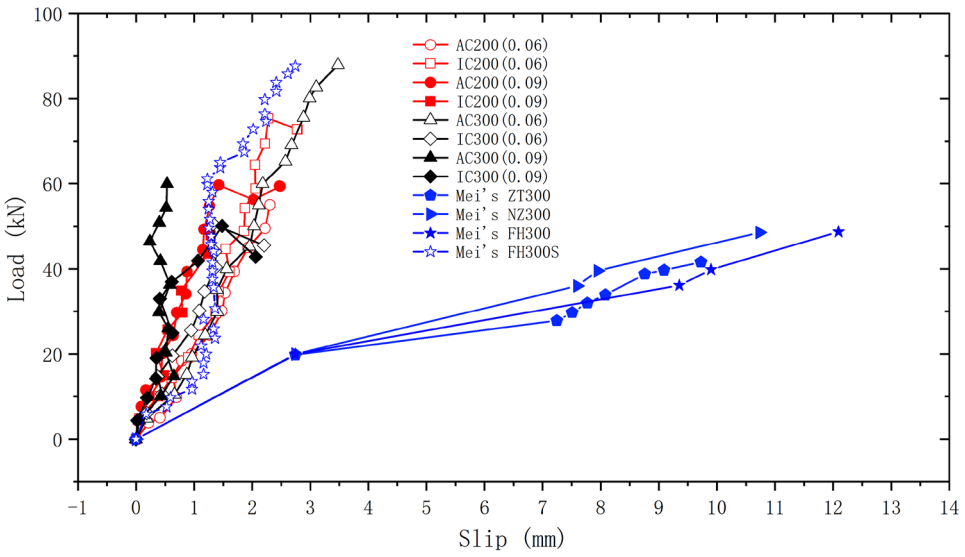

Fig. 7 Load – slip curves of each anchorage

during loading causes the tendons to be squeezed tighter, so the slope of the load–slip curve is greater.

3.3 Stress analysis of CFRP tendon

In addition to the load–slip curve, the stress distribution of CFRP tendon is also the objectives of tension test. The stress distribution can intuitively reflect the difference between arcuate-cone anchorage and inner cone anchorage. It can also be verified whether the arcuate-cone anchorage can achieve the desired results in design, i.e. whether it can alleviate the stress concentration and reduce the peak stress.

In the bond type anchorage, the stress statues of the tendons and the colloid is shown in Fig. 8. Based on the equilibrium condition, the horizontal force can be derived according to the following equation.

$$\frac{dT_x}{dx} = 2\pi r_t \tau_x,$$

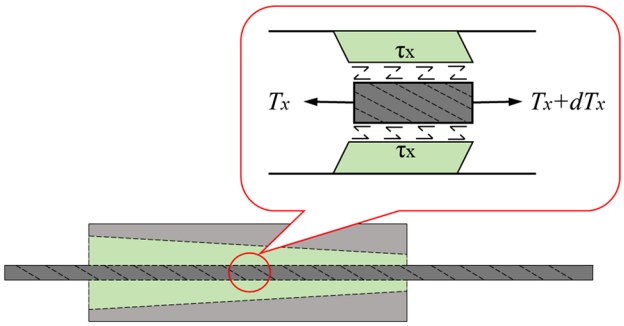

Fig. 8 Stress sketch of the infinitesimal element of the tendon and the colloid

where x is the length of the free end, T_x is the axial force of the CFRP tendons at x, r_t is the radius of the CFRP tendons, τ_x is the shear stress at x. As shown in Fig. 8, the shear stress on the surface of the tendon τ_x, representing the interfacial bond stress, is proportional to the slope of the $T_x - x$ curve. In other words, the interfacial bond stress is proportional to the axial stress of the CFRP tendons. Since the shear stress τ_x is difficult to obtain, a series of strain gauges were arranged on the surface of the tendons. The experimentally obtained axial stress of the tendons was used to indirectly reflect the distribution of the shear stress. Figure 9 shows the location of the strain gauges inside the anchorages.

Take a pair of inner cone and arcuate-cone anchors with the same parameters as an example. The stress distribution curves of IC200(0.06) and AC200(0.06) are shown in Fig. 10. The legend of the same shape represents the stress distribution curve of different anchor types under the same load level. Compared with the traditional inner-cone anchorage, it can be seen that the peak stress of arcuate-cone anchorage is significantly reduced and transferred to the interior of the anchor zone. In addition, the stress distribution of arcuate-cone anchorage is uniform in the whole bond length. For different load levels, the greater the load, the more obvious the effect of arcuate-cone anchorage on relieving stress concentration.

To verify the effect of anchorage shape on the stress concentration phenomenon, the 2D axisymmetric finite element models of inner cone and arcuate-cone anchorages were established using the ABAQUS program. Since the finite element model is a two-dimensional axisymmetric model, the element type of the present model is CAX4R. The model consists of three parts: the anchor cup, the colloid and the tendon. In normal operation, the colloid–tendon interface (blue line in Fig. 11) does not have a relative slip. Therefore, the tendon and the colloid were bound by

(a) Strain gauge location on the surface of CFRP tendons (bond length of 200mm)

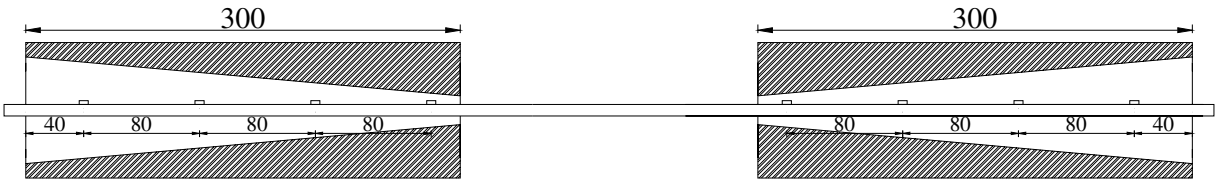

(b) Strain gauge location on the surface of CFRP tendons (bond length of 300mm)

Fig. 9 **a** Strain gauge location on the surface of CFRP tendons (bond length of 200 mm), **b** Strain gauge location on the surface of CFRP tendons (bond length of 300 mm)

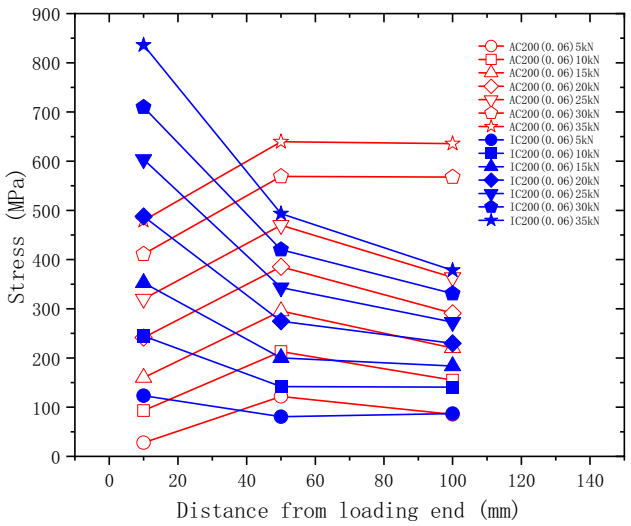

Fig. 10 Stress distribution curves of IC200(0.06) and AC200(0.06)

tie in ABAQUS. The anchor cup–colloid interface (orange line in Fig. 11) allows relative slip to squeeze the colloid and thus anchor the tendon. Therefore, the two surfaces were connected by penalty in ABAQUS. The boundary conditions were simulated by constraining the displacement of the end of the anchor cup (red line in Fig. 11).

The loading condition of the anchor was simulated by applying a 10 mm displacement at the tendon end. The distributions of shear stresses for inner cone and arcuate-cone anchorages with same size were shown in Fig. 12. Figure 12a illustrates the stress distribution within the inner cone anchorage, and it can be found that the stresses were concentrated in a very small area at the end. In contrast, the stresses within the arcuate-cone anchorage in Fig. 12b were uniformly distributed over a large area. According to the results of the FEM analysis, the peak stress of the arcuate-cone anchorage was reduced by 61.5% compared to the inner cone under the current loading conditions. Therefore, the change in cone shape would have an effect on the stress distribution within the anchor.

4 Analysis of monitoring data

4.1 Analysis of conventional AE parameters

There is a certain relationship between the parameters of the AE signal. Figure 13 shows the two-dimensional correlogram distribution of the amplitude with signal energy, and the amplitude with center frequency during the loading process of the specimen.

The energy and center frequency of the acoustic emission signal both show a certain distribution pattern with the variation of the amplitude. The energy distribution diagram shows that a few signals have extremely high energy. The energy of these high-energy signals is several orders of magnitude different from that of general signals, and their amplitudes are approximately equal to 100 dB. Similarly, the amplitude of most signals is concentrated below 70 dB, and the signal center frequency shows a decreasing trend with an increase in the amplitude. These distribution patterns are commonly found among specimens with different failure modes.

4.2 Identification of anchorage's failure modes

To identify the failure modes of the anchorages, a series of analyses were performed based on the acoustic emission monitoring results. Three different failure modes are shown in Fig. 6, which are pull-out failure, partial debonding failure and tensile fracture of CFRP tendons. Obviously, the failure modes are closely related to the shear failure of the tendon-colloid interface. And whether the damage occurring in the anchorage is a tensile crack or a shear crack can be determined by the RA-AF analysis method.

The RA-AF analysis method defines two parameters of the rise angle (RA) and the average frequency (AF) of the acoustic emission signal, calculated as follows.

$$he\ rise\ angle = the\ rise\ time/the\ maximum\ amplitude$$

$$the\ average\ frequency = the\ AE\ counts/the\ duration\ time$$

Such some AE parameters as count, maximum amplitude, duration time and rise time as shown in Fig. 14.

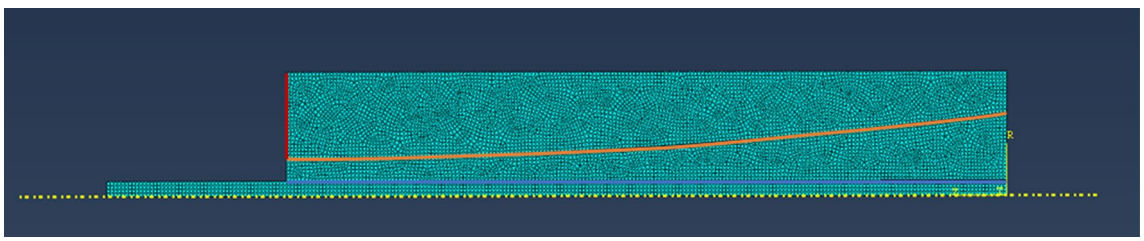

Fig. 11 Boundary conditions and interactions of FEM

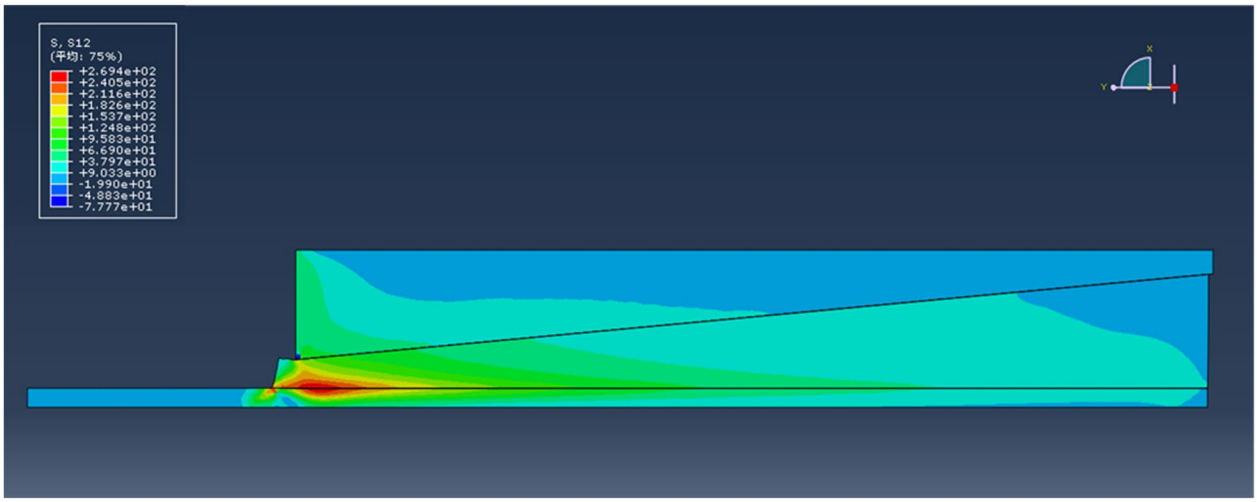

(a) Inner-cone anchorage

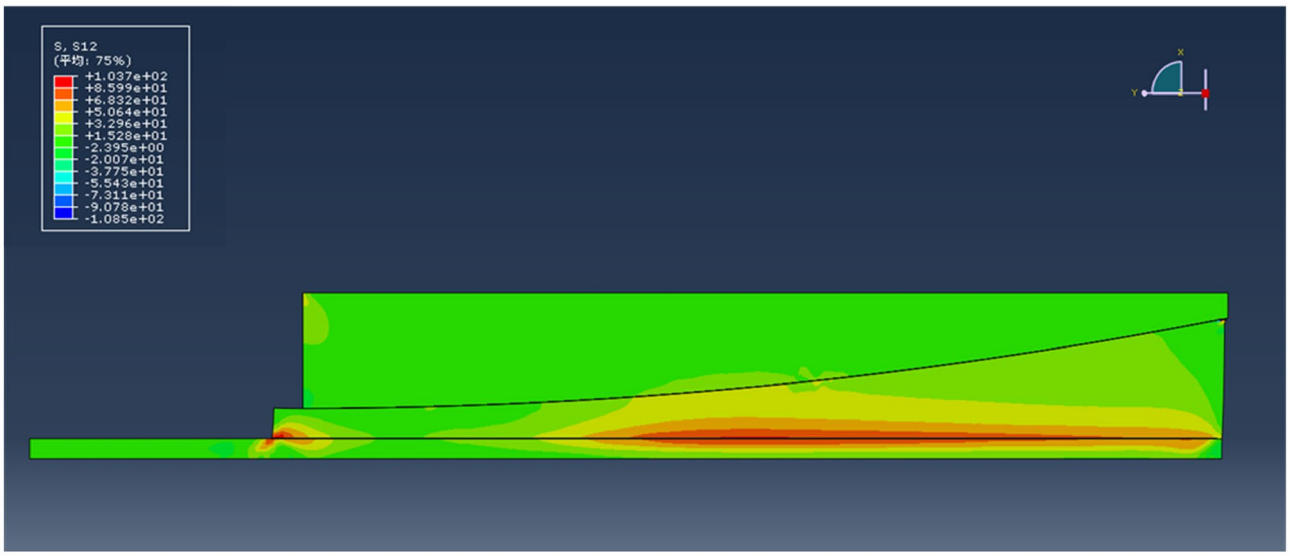

(b) Arcuate-cone anchorage

Fig. 12 Stress distribution by FEM analysis

The RA-AF analysis has been widely used in the field of acoustic emission monitoring as a simple and accurate signal processing method to distinguish tension cracks from shear cracks. Because of the characteristics of short rise time, short duration, and large amplitude of tension cracks, RA is lower than AF, while shear cracks have a long duration and have lower AF and higher RA values. Therefore, by making a scatter plot of RA and AF for each signal, the signals corresponding to tensile cracks show a different distribution from those corresponding to shear cracks. The acoustic emission signals corresponding to these two different types of cracks can be distinguished by a dividing line, as shown in Fig. 15.

The number of damages in the bonded anchorages was so large that more than a thousand signals were obtained during the monitoring of each specimen. Therefore, it was necessary to perform a statistical analysis of the AE signals. Through the analysis of acoustic emission parameters in Sect. 4.1, it was found that the energy and center frequency both show a certain distribution pattern with the variation of the amplitude. Therefore, the classification of signals by their amplitude allows them to be categorized into several classes with different characteristics.

To analyze the relationship between the monitoring data and failure modes, the AE signals during the test process are classified into five categories: Class1 (50−60 dB), Class2

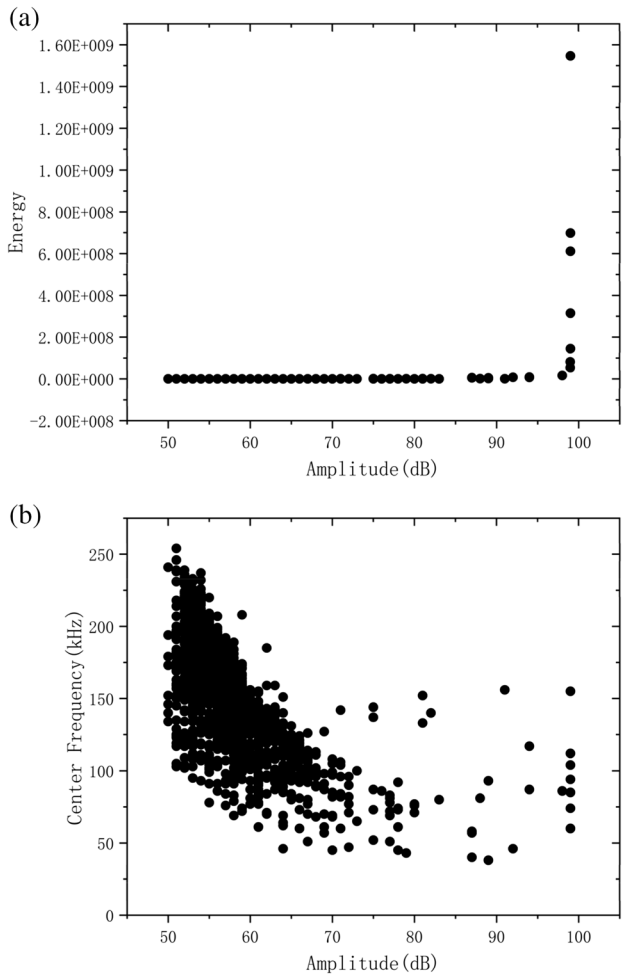

Fig. 13 AE features correlation distribution for IC200(0.09): **a** amplitude−energy distribution, **b** amplitude−center frequency distribution

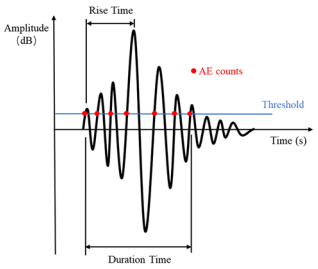

Fig. 14 AE parameters of a single AE signal

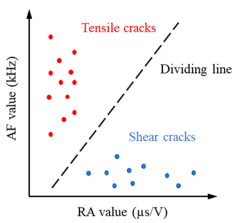

Fig. 15 Crack classification based on RA-AF method

(60 – 70 dB), Class3 (70 – 80 dB), Class4 (80 – 90 dB), and Class5 (90 – 100 dB). Data such as the percentage of signal to total signal, percentage of signal energy to total energy, and average peak frequency of the five types of signals are shown in Tables 4, 5 and 6; Fig. 16.

The energy of the acoustic emission signal represents the severity of the damage that produced it. As can be seen in Fig. 16, the percentage of each class's signal number rapidly decreases with an increase in amplitude, but the proportion of energy rapidly increases. Among them, signals in Class1 have the largest percentage, accounting for 70–80% of the total signals, but its energy contribution is approximately 0.05%, which is caused by a large number of slight damages. In contrast to Class1, the number of signals in Class5 accounts for approximately 1% of the total signals, but the proportion of energy is as high as 99%. These signals are produced by a few extremely serious injuries. This extreme distribution proves that the number of signals produced by the failure of the CFRP-bonded anchorage is small, and the failure of the anchorage is instantaneous and unpredictable.

The acoustic emission results are not the same for specimens with different failure modes, and a correlation between the failure modes and the acoustic emission results can be established by RA-AF analysis.

The energy of the signals represents the damage severity. Therefore, signals with different energies have different importance. Tables 4, 5 and 6 show that the signals caused by minor damages (Class 1 to 4) has a lower RA value and relatively higher AF value. According to the principles of RA-AF analysis, the crack type is a tensile crack with a short rise time. For specimens with different failure modes, the signals caused by minor damages did not show differences.

For signals caused by serious damages in Class5, the RA and AF values of the three specimens are significantly different. For specimens whose failure mode is pull-out failure, such as IC200 (0.09), the RA value of the signal in Class5 is greater than the AF value, which indicates that a serious shear damage occurred. This is consistent with the failure mode obtained from the tests, i.e., shear failure at the tendon-colloid interface.

The RA value of the high-energy signal generated when testing specimens whose failure mode is tensile fracture, such as AC300(0.06), is less than the AF value, which proves that no dangerous interfacial shear crack occurs.

Specimens whose failure mode is partial debonding failure, such as AC200 (0.09), is between the aforementioned two kinds of specimens, the values of RA and AF of the AE signal in Class5 are similar.

The RA-AF distribution of the high-energy acoustic emission signals of the three specimens is shown in Fig. 17. According to the principle of RA-AF analysis, the points with lower RA values in Fig. 17 represent tension cracks. The colloids in all anchorages will be squeezed to produce

Table 4 Statistical analysis of IC200(0.09) AE features

AE feature	Amplitude (dB)	Energy	Peak frequency (kHz)	RA (μs/V)	AF (kHz)	Signal number contribution (%)	Energy contribution (%)
Class1	55.22	1841.23	48.12	10.19	48.77	68.45	0.05
Class2	62.86	9452.78	45.28	11.71	36.54	26.12	0.09
Class3	73.39	1.49E+05	40.66	31.11	23.63	3.41	0.19
Class4	83.79	1.91E+06	35.57	10.31	21.13	1.09	0.76
Class5	96.83	2.91E+08	46.42	32.69	19.09	0.93	98.92

Table 5 Statistical analysis of AC200(0.09) AE features

AE feature	Amplitude (dB)	Energy	Peak frequency (kHz)	RA (μs/V)	AF (kHz)	Signal number contribution (%)	Energy contribution (%)
Class1	54.58	1040.18	60.10	3.53	58.93	82.31	0.04
Class2	62.63	8160.02	58.83	9.12	44.05	15.34	0.07
Class3	74.88	1.38E+05	56.41	10.32	32.86	1.29	0.09
Class4	83.43	1.42E+06	45.57	1.98	26.85	0.53	0.39
Class5	95.29	3.59E+08	42.57	17.25	18.03	0.53	99.40

Table 6 Statistical analysis of AC300(0.06) AE features

AE feature	Amplitude (dB)	Energy	Peak frequency (kHz)	RA (μs/V)	AF (kHz)	Signal number contribution (%)	Energy contribution (%)
Class1	54.69	1167.81	58.51	6.00	66.29	74.57	0.03
Class2	62.92	8028.98	57.27	7.53	47.91	20.51	0.06
Class3	73.26	1.32E+05	54.28	7.14	30.44	3.06	0.15
Class4	84.00	1.57E+06	40.12	2.84	25.34	0.70	0.42
Class5	95.93	2.28E+08	29.39	9.61	16.65	1.16	99.34

tension cracks. Therefore, all specimens will have points representing tension cracks in Fig. 17.

In Fig. 17, the points with high RA values and low AF values are produced by shear cracks. It can be seen that severe shear damage was present in IC200 (0.09) whose failure mode is pull-out failure, and not in AC300 (0.06) whose failure mode is tensile fracture. In the tension test, a single serious shear damage would cause the anchorage to fail. Therefore, only one shear crack could be collected, that is, only one point representing shear crack in Fig. 17. Thus, there are indications that the presence or absence of points representing shear cracks is related to different failure modes.

According to the above crack classification results, the difference in RA-AF values of the high-energy signals showed a correlation with the failure modes of bonded anchorages.

4.3 Damage evolution based on accumulated energy

During the test of CFRP tendon bonded anchorage from tension to failure, each anchorage accumulated multiple damages and produced a large number of AE signals. In acoustic emission monitoring, the energy represents the severity of the damage and the count represents the activity of the acoustic emission. To understand the damage evaluation of different specimens during the test, Figs. 18, 19 and 20 shows the loading history curve versus the count and the cumulative energy curves of the AE signals.

The accumulation of energy means that the damage in the anchorage is gradually increasing. According to the energy accumulation curves and the count curves in Figs. 18, 19 and 20, the damage process of each specimen can be divided into three stages: contact stage, sliding elastic stage, and damage

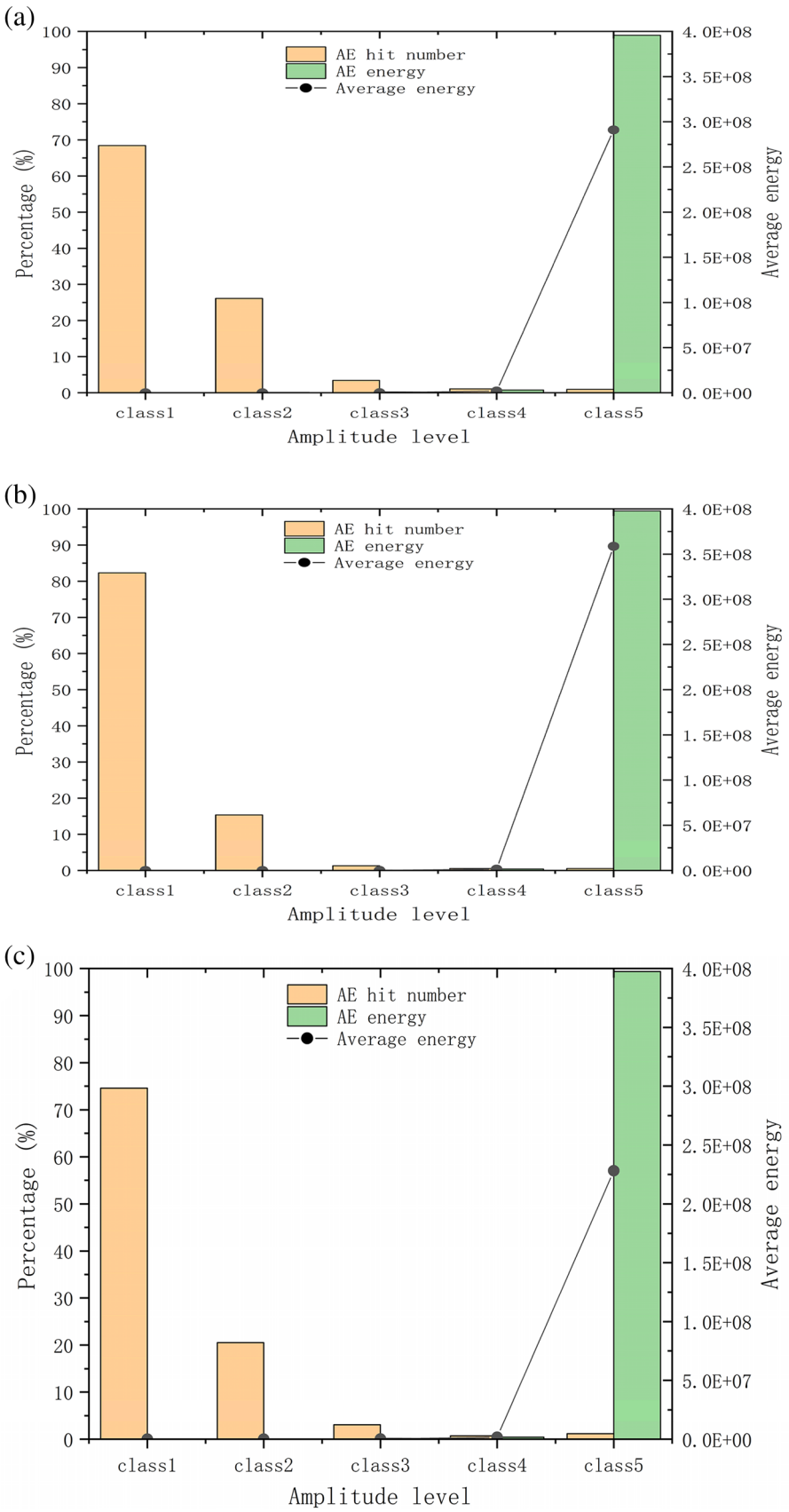

Fig. 16 Histogram of statistical signal number and corresponding energy contribution: **a** IC200(0.09) **b** AC200(0.09) **c** AC300(0.06)

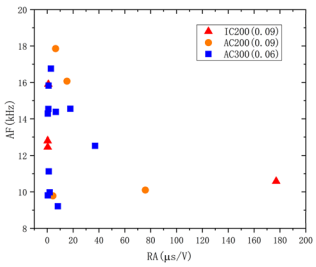

Fig. 17 RA-AF distribution of high-energy acoustic emission signals

plastic stage. The contact stage refers to the first increase in the energy accumulation value from the beginning of loading, during which a small amount of AE energy is generated owing to the contact between the components of the test device. The sliding elastic stage and damage plastic stage are bounded by the first sharp increase in the accumulated energy in the middle and later phases of loading. In the sliding elastic stage, there is no accumulation of AE energy, i.e., the damage intensity is very small, and the slight damage has little contribution to the failure of the specimen. In the damage plastic stage, serious damage occurs, and the cumulative AE energy increases exponentially. The count represents the activity of the acoustic emission. As can be seen in Figs. 18, 19 and 20, the increases in cumulative energy are accompanied by larger counts. It can be indicated that severe damage is consistent with active acoustic emission.

Moreover, the growth of the energy accumulation value shows a ladder type, and the energy is mainly generated by

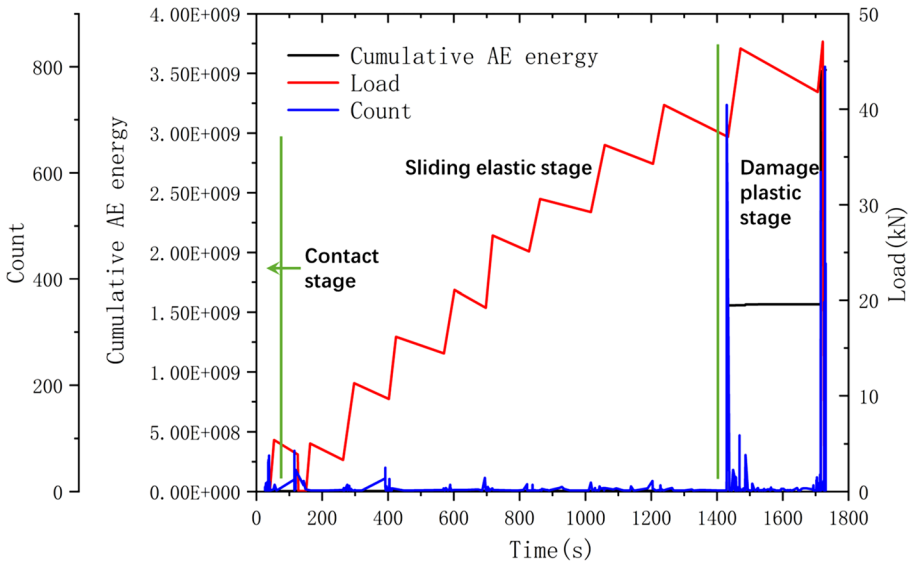

Fig. 18 Loading history versus AE features for IC200(0.09)

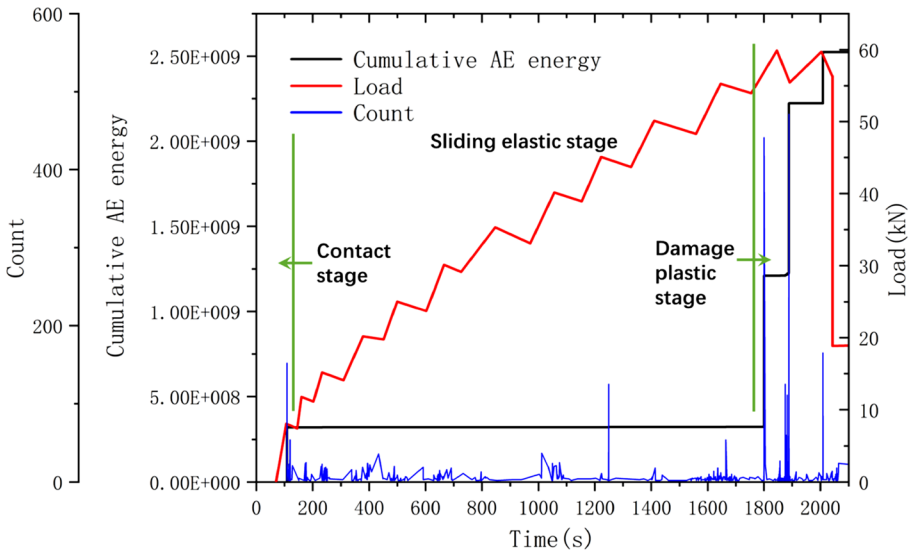

Fig. 19 Loading history versus AE features for AC200(0.09)

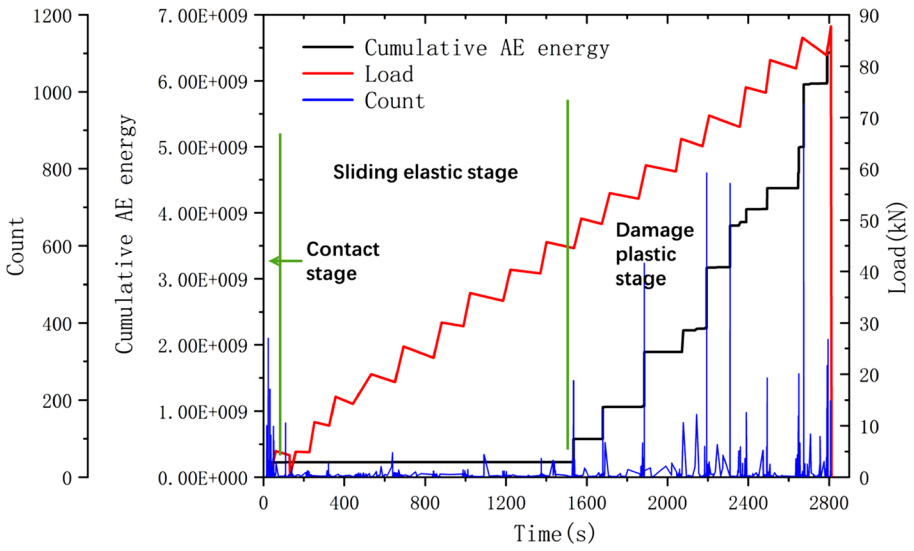

Fig. 20 Loading history versus AE features for AC300(0.06)

a few high-energy signals. When compared with other large number of signals, the energy value of these signals is different with several orders of magnitude. In other words, the failure of the bond-type anchorage is mainly caused by a few serious damages, and is sudden.

4.4 Discussion on failure mechanisms

The inner cone and arcuate-cone anchorages can be collectively called cone-type bonded anchorages. The principle of cone-type bonded anchorages is combining the chemical bonding force between CFRP and adhesives with the extrusion force produced by colloidal compression. Therefore, the sum of the two forces is the anchoring capacity.

The colloidal extrusion force is generated with the relative slip between the colloid and the barrel, as shown in Fig. 21a. Both tension test results and acoustic emission monitoring confirmed that relative slip of the colloid to the sleeve occurred in cone-type bonded anchorages. All specimens in the present tensile test had relative slips at the barrel–colloid interface, as shown in Fig. 21b. The damage process was obtained from the analysis of the acoustic emission monitoring data in Figs. 18, 19 and 20 above, where the sliding elastic stage without damage proves that the slip occurs at the barrel–colloid interface.

The ultimate chemical bonding force between tendons and adhesives is constant for anchors with a determined length, while the extrusion force generated by colloid extrusion increases with the loading process. Hence, it can be presumed that different extrusion force increments may lead to different failure modes.

First, when the colloid is not squeezed or the increment of the colloid extrusion force is very small, only the chemical bonding force plays an anchoring role. Along with the loading process, when the load value reaches the maximum

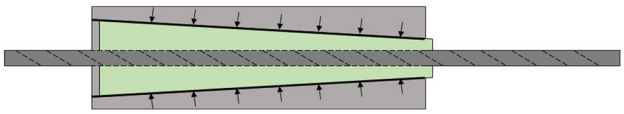

(a) Schematic diagram of relative slip

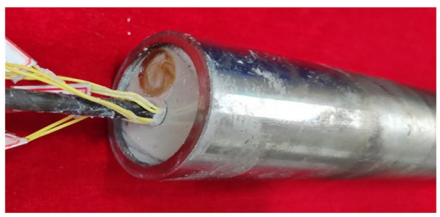

(b) Relative slip in the tested specimen

Fig. 21 The relative slip of the colloid to the sleeve

chemical bonding force, the tendon is pulled out from the colloid. This failure mode is pull-out failure, and its principle is shown in Fig. 22a.

Second, during the loading process of the anchorage, the colloidal extrusion force continuously increased with the loading process, but its growth rate was slow. When the load exceeds the sum of the colloidal extrusion force and chemical bonding force at a certain time, partial debonding occurs at the interface between the tendon and colloid, and the CFRP tendon and part of the colloid are pulled out of the barrel. This failure mode is partial debonding failure, and its principle is shown in Fig. 22b.

Third, during the loading process of the anchorage, the extrusion force increment increases rapidly with the loading process, or because of the longer length of the anchorage, the ultimate chemical bond force is larger. Hence, the load cannot exceed the sum of the colloidal extrusion force and chemical bonding force. The load increases continuously until the CFRP tendon is broken. This failure mode is tensile

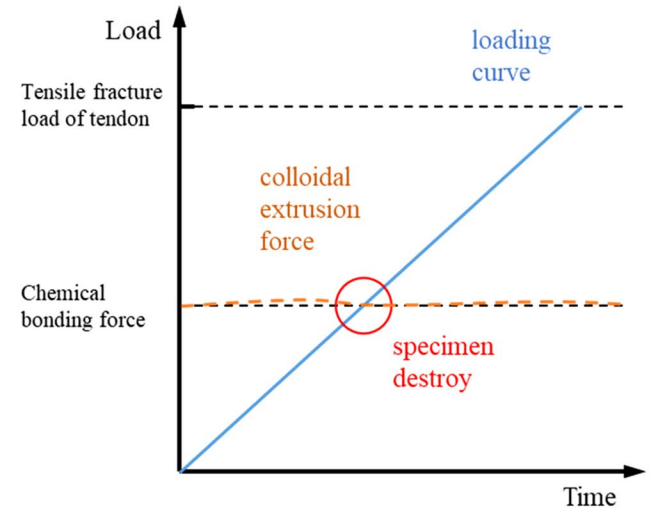

(a) Principle of pull-out failure

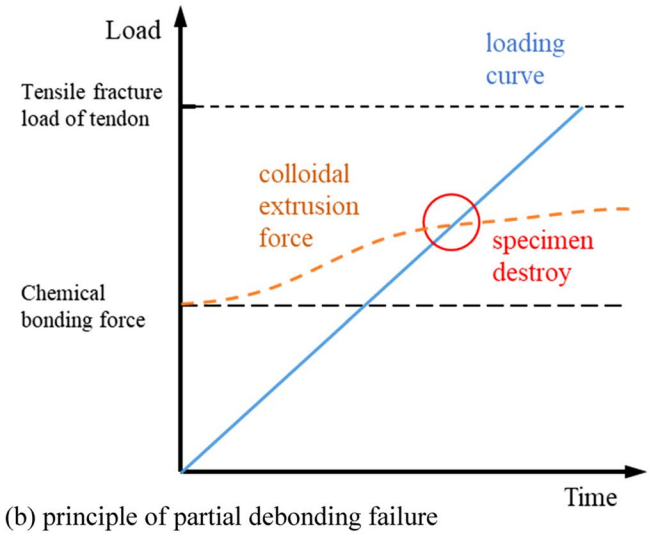

(b) principle of partial debonding failure

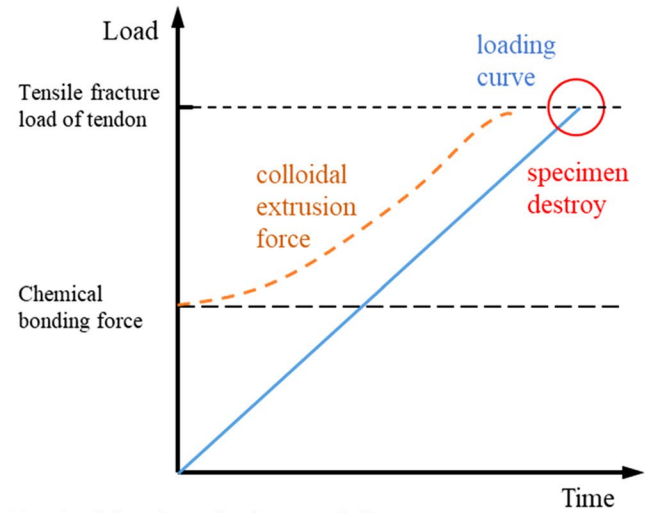

(c) principle of tensile fracture failure

Fig. 22 Schematic diagrams of three failure modes

fracture of the CFRP tendons, and the principle is shown in Fig. 22c.

5 Conclusion

In this study, a novel bonded anchorage was designed to relieve the stress concentration phenomenon. Furthermore, this investigation firstly applied acoustic emission monitoring technique to bonded anchorages to obtain damage information inside the anchorages. The following conclusions can be drawn:

(1) The load–slip relationship of bonded anchor is nonlinear, and the slippages of CFRP tendons increase significantly near the ultimate bearing capacity.
(2) Changing the cone to a curved shape can relieve the stress concentration, and the peak stress can be reduced by 61.5% according to the present FEM results.
(3) There are some indications that the RA-AF analysis results of the high-energy signals are related to different failure modes of anchorages.
(4) The damage process of bond type anchorage can be divided into contact stage, sliding elastic stage, and damage plastic stage.

Acknowledgements This work was supported by the National Key R&D Program of China [Project No. 2018YFC1505302]; National Natural Science Foundation of China (NSFC) [grant numbers No. 51778104]; and the Fundamental Research Funds for the Central Universities [Project No. DUT19LAB26].

References

1. Huang P, Sun Y, Mei K, Wang T (2020) A theoretical solution for the pullout properties of a single FRP rod embedded in a bond type anchorage. Mech Adv Mater Struct 27:304–317
2. Wang X, Wu Z (2009) Integrated high-performance thousand-metre scale cable-stayed bridge with hybrid FRP cables. Compos B: Eng 41:166–175
3. Puigvert F, Crocombe AD (2014) Gil L (2014) Static analysis of adhesively bonded anchorages for CFRP tendons. Constr Build Mater 61:206–215
4. Mei K, Seracino R, Lv Z (2016) An experimental study on bond-type anchorages for carbon fiber-reinforced polymer cables. Constr Build Mater 106:584–591
5. Campbell TI, Shrive NG, Soudki KA, Al-Mayah A, Keatley JP, Reda MM (2000) Design and evaluation of a wedge-type anchor for fibre reinforced polymer tendons. Can J Civ Eng 27:985–992
6. Meier U, Farshad M (1996) Connecting high-performance carbon-fiber-reinforced polymer cables of suspension and cable-stayed

bridges through the use of gradient materials. J Comput Aided Mater Des 3:379–384
7. Mei K, Sun S, Li B, Sun Y, Jin G (2018) Experimental investigation on the mechanical properties of a bond-type anchor for carbon fiber reinforced polymer tendons. Compos Struct 201:193–199
8. Mei K, Sun Y, Sun S, Ren X, Zhao J (2020) Experimental investigation on the mechanical properties of a novel anchorage for carbon fiber reinforced polymer (CFRP) tendon. Compos Struct 234:111704
9. Schmidt JW, Bennitz A, Täljsten B, Goltermann P, Pedersen H (2012) Mechanical anchorage of FRP tendons – a literature review. Constr Build Mater 32:110–121
10. Sayed-Ahmed EY, Shrive NG (1998) A new steel anchorage system for post-tensioning applications using carbon fibre reinforced plastic tendons. Can J Civ Eng 25:113–127
11. Schesser D, Yang QD, Nanni A, Giancaspro JW (2014) Expansive grout-based gripping systems for tensile testing of large-diameter composite bars. J Mater Civ Eng 26:250–258
12. Hodhod H, Uomoto T (1992) Effect of state of stress at the grips and matrix properties on tensile strength of CFRP rods. Doboku Gakkai Ronbunshu 451:245–253
13. Al-Mayah A, Soudki K, Plumtree A (2013) Simplified Anchor System for CFRP Rods. J Comps Constr. https://doi.org/10.1061/(ASCE)CC.1943-5614.0000367
14. Du F, Pan S, Li D (2018) Damage evaluation and failure mechanism analysis of steel tube confined reinforced-concrete columns by acoustic emission technology. Lat Am J Solids Struct. https://doi.org/10.1590/1679-78255339
15. Zitto ME, Piotrkowski R, Gallego A, Sagasta F, Benavent-Climent A (2015) Damage assessed by wavelet scale bands and b-value in dynamical tests of a reinforced concrete slab monitored with acoustic emission. Mech Syst Signal Process 60–61:75–89
16. Li D, Du F, Ou J (2017) Damage evaluation of fiber reinforced plastic-confined circular concrete-filled steel tubular columns under cyclic loading using the acoustic emission technique. Smart Mater Struct 26:035014
17. Drummond G, Watson JF, Acarnley pp. (2007) Acoustic emission from wire ropes during proof load and fatigue testing. NDT E Int 40:94–101
18. Liu S, Wu C, Zhou J, Liu T, Zhuang S, Luo Y, Yang X (2020) Relation between the shear stress distribution and the resulting acoustic emission variation in concrete beams. Struct Control Health Monit 27:e2528
19. Abouhussien AA, Hassan AAA (2017) Acoustic emission-based analysis of bond behavior of corroded reinforcement in existing concrete structures. Struct Control Health Monit 24:e1893
20. Behnia A, Chai HK, Ranjbar N, Jumaat MZ (2016) Damage detection of SFRC concrete beams subjected to pure torsion by integrating acoustic emission and Weibull damage function. Struct Control Health Monit 23:51–68
21. Vidya SR, Raghu PBK, Singh RK (2015) Kaiser effect observation in reinforced concrete structures and its use for damage assessment. Arch Civ Mech Eng 15:548–557
22. Philippidis TP, Assimakopoulou TT (2008) Using acoustic emission to assess shear strength degradation in FRP composites due to constant and variable amplitude fatigue loading. Compos Sci Technol 68:840–847
23. Chelliah SK, Kannivel SK, Vellayaraj A (2019) Characterization of failure mechanism in glass, carbon and their hybrid composite laminates in epoxy resin by acoustic emission monitoring. Nondestruct Test Eval 34:254–266
24. Ghaib M, Shateri M, Thomson D, Svecova D (2018) Study of FRP bars under tension using acoustic emission detection technique. J Civ Struct Health Monit 8:285–300
25. Al-Mayah A, Soudki K, Plumtree A (2001) Experimental and analytical investigation of a stainless steel anchorage for CFRP prestressing tendons. PCI J 46(2):88–99
26. Zhang B, Benmokrane B, Chennouf A (2000) Prediction of tensile capacity of bond anchorages for FRP tendons. J Compos Constr 4(2):39–47
27. Huang P, Sun Y, Mei K et al (2020) A theoretical solution for the pullout properties of a single FRP rod embedded in a bond type anchorage. Mech Adv Mater Struct 27(4):304–317